



M Ű E G Y E T E M 1 7 8 2

**Budapest University of Technology and Economics**  
Faculty of Electrical Engineering and Informatics  
Department of Automation and Applied Informatics

# THESIS BOOKLET

**Static and Dynamic Behavior Optimization of  
Dual Active Bridge Converters**

SZABOLCS VERÉB

Supervisor:  
István Varjasi, Ph.D.

Budapest, 2026



# 1 Introduction, objectives

Nowadays, global electricity consumption is growing rapidly, and with the widespread use of electric vehicles, this trend is expected to continue. The spread of renewable electric power sources is increasing the demand for energy storage solutions. Most of these devices require galvanically isolated, high-power, high-efficiency, bidirectional DC-DC converters, which typically use a dual active bridge (DAB) topology.

This type of DC-DC converter can be operated efficiently if the ratio of the primary and secondary DC voltages is close to the transformer's turns ratio. Numerous publications are available on the control of DAB converters. The advantage of Single Phase Shift (SPS) control is that a single parameter can be used to control the total power flowing through the device, resulting in a simple control algorithm. The literature deals with more complex solutions in many cases, such as Dual Phase Shift (DPS) or Triple Phase Shift (TPS), but their practical applicability is questionable, as it is not trivial to select the ideal combination from the multiple intervention options during operation. A significant part of the publications deals with increasing efficiency (reducing circulating current, extending ZVS operation), while the dynamic behavior of the converter and the effects of switching dead times are rarely mentioned.

During my research, I looked for control structures that improve the transient behavior of SPS-controlled DAB converters with additions, without major modifications. With today's low-cost digital programmable devices (DSP, FPGA, SoC), computing capacity is no longer a limitation, and algorithms that were previously impractical are now becoming feasible.

## 2 Research methodology

The DAB converter consists of two complete semiconductor transistor bridges (usually MOSFET or IGBT) and a transformer (see Figure 1). This type of converter is capable of bidirectional power flow and also provides galvanic isolation. In practice, it is generally used at medium and high power levels due to its high number of semiconductors.

My research is related to the FIEK 16-1-2016-0007 project, within the framework of which a high-performance test laboratory was built. The built-in equipment includes a 360 kW DAB converter, which I was able to use to test and apply the results of my research.

I began my research by reviewing the literature, then interpreted the time functions of the converter, based on which I wrote down and interpreted the equations describing the operation from the perspective of the phenomenon and problem under investigation. I then derived the solutions analytically in mathematical form. As a next step, I created a model of the

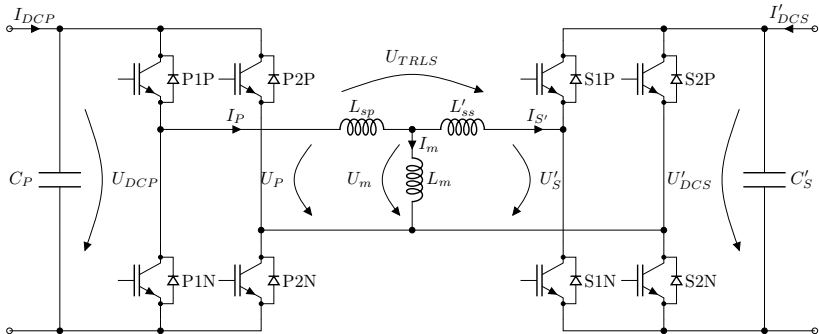


Figure 1: DAB converter power circuit schematic.

DAB converter in the MATLAB Simulink environment, which allowed me to test the solutions in an offline simulation environment. When a promising solution was found, I continued my work with hardware-in-the-loop (HIL) simulation. I discretized the main circuit model and ported it to an FPGA-based development board, and implemented the algorithms on a DSP-based control card. After achieving satisfactory results, the solutions were tested on real equipment.

### 3 Summary of new scientific findings

I have summarized the results of my research in three theses.

The first deals with the static behavior of SPS-controlled DAB converters. I developed a control method that is capable of eliminating transformer current anomalies caused by voltage measurement errors occurring in practical applications. I demonstrated how switching dead time affects converter operation and developed an adaptive dead time compensation method.

In my second thesis, I deal with the dynamic behavior of SPS-controlled DAB converters. I have developed two types of current control methods that improve the behavior of the converter during transients (e.g. when the input voltage or load current changes) by means of in-period interventions. I have shown that switching dead time can cause significant errors in the operation of the controller and have developed an adaptive dead time compensation method.

The third thesis deals with the start-up transients of DAB converters. Usually, one DC bus operates with constant voltage (e.g. a battery pack is connected to it), while the load is connected to the other bus. When starting the DAB converter, care must be taken to ensure that the uncharged capacitor on the load side of the DC bus is first charged in a controlled manner. Only then can normal operation of the converter begin. I have

developed a precharge method that allows the converter to start up with current limiting and a constant switching frequency in a short time, even with varying initial conditions.

---

**1 Thesis.** [J1] [B1] [J2] [C1] *I have proposed two new control methods, which improves the static behavior of SPS controlled DAB converters. With the ripple current control (RCC) algorithm, leveraging current rate of change feedback, the current stress (caused by errors in the DC voltage measurement) is significantly reduced, thus improving the converter efficiency. I have shown that the switching dead time is causing discontinuous current conduction in SPS controlled DAB converters. I have introduced a novel adaptive dead time compensation (ADTC) logic, which eliminates the unwanted effects of switching dead time.*

---

In practical applications, SPS control is most commonly used. The switching waveforms are shown in Figure 2. The voltages ( $U_P$  and  $U_S$ ) of the primary and secondary windings of the transformer are square waves with a duty cycle of approximately 50%. The phase shift ( $\tau$ ) set between them determines the voltage-time area on the transformer's stray inductance, and thus the change in the transformer's primary current, which is closely related to the power transferred in the next period.

$$\Delta I_P = \frac{U_{DCP} + U'_{DCS}}{L_{sp} + L'_{ss}} \cdot \tau \quad (1)$$

The PWM carrier signal is a sawtooth signal with a frequency six times higher than the carrier frequency and a value range of [0,1]. During SPS control, we intervene in the 1st and 4th carrier signal periods.

A cascade control structure is typically used to control the transformer current and DC voltages. A typical control loop is shown in Figure 3. The internal control loop is responsible for current control. The external loop regulates the difference between the DC bus voltages to the value corresponding to the reference signal. The current and voltage signals of the converter are sampled twice within a switching period, at times C1 and C2 in Figure 2. The code section implementing the digital control loop is executed after sampling. The switching operations are performed symmetrically with respect to the center of the sawtooth carrier. The outputs of the controllers ( $d_m$  and  $d_0$ ) are interpreted in proportion to the carrier signal period (0...1). The comparison values for the switching operations are summarized in Table 1. The following relationship exists between the set phase delay and the output  $d_0$  of the controller:

$$\tau = d_0 \cdot T_C = d_0 \cdot \frac{T_{SW}}{6} \quad (2)$$

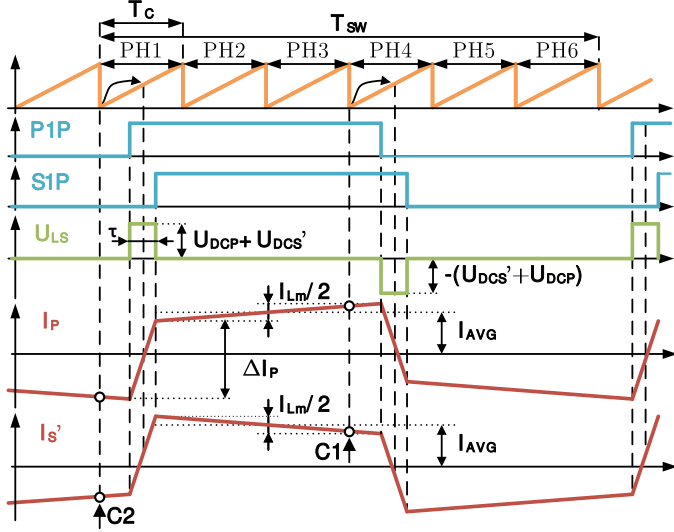


Figure 2: Typical switching waveforms of a SPS controlled DAB converter.

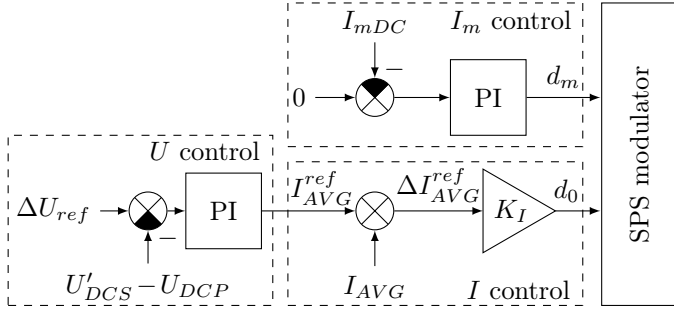


Figure 3: Typical controller of a SPS controlled DAB converter.

Table 1: The switching table of the SPS modulator.

Primary	C2	C1	Secondary	C2	C1
P1 to $U_{DCP}$	$\frac{1-d_0}{2} - d_m$	x	S1 to $U_{DCS}$	$\frac{1+d_0}{2} - d_m$	x
P1 to 0	x	$\frac{1-d_0}{2} + d_m$	S1 to 0	x	$\frac{1+d_0}{2} + d_m$
P2 to $U_{DCP}$	x	$\frac{1-d_0}{2} + d_m$	S2 to $U_{DCS}$	x	$\frac{1+d_0}{2} + d_m$
P2 to 0	$\frac{1-d_0}{2} - d_m$	x	S2 to 0	$\frac{1+d_0}{2} - d_m$	x

The voltage is controlled by a PI controller, while two controllers are used for the transformer current. The DC component of the magnetizing current of the transformer is controlled by a slow PI controller (*I<sub>m</sub> control*). The DC component of the magnetizing current is calculated from the samples of the primary and secondary currents of the transformer.

$$I_{mDC}[n] = \frac{I_P[n] - I'_S[n]}{2} + \frac{I_P[n-1] - I'_S[n-1]}{2} \quad (3)$$

In accordance with the output of the regulator  $d_m$ , we increase the width of the positive voltage pulse reaching the transformer and decrease the negative one. If  $d_m \neq 0$ , then the voltage-time area across the magnetizing inductance will not be zero within one switching period, i.e., the average value of the magnetizing current of the transformer will change.

The total power flowing through the transformer can be controlled by changing the current every half cycle. The average current required for feedback can be calculated from the primary and secondary currents of the transformer.

$$I_{AVG}[C1] = \frac{I_P[C1] + I'_S[C1]}{2} \quad I_{AVG}[C2] = -\frac{I_P[C2] + I'_S[C2]}{2} \quad (4)$$

The required phase shift ( $d_0$ ) is determined from the desired average current change of the transformer ( $\Delta I_{AVG}^{ref}$ ) multiplied by  $K_I$ .

$$K_I = \frac{\tilde{L}_{sp} + \tilde{L}'_{ss}}{U_{DCP} + U'_{DCS}} \cdot \frac{1}{T_{PWM}} \quad (5)$$

Typically, the transformer has relatively low stray inductance, allowing the converter to operate with good dynamic characteristics. However, this also means that the voltage difference between the two DC rails can result in large current changes even when the primary and secondary voltages of the transformer are of the same polarity. In some applications, even if the DC voltages on the primary and secondary sides are regulated to the same value, unwanted transformer waveforms are obtained. This is typically caused by a voltage measurement error, for example if the DC bus has ohmic resistance between the capacitor bank and the transformer terminals. In this case, the amplitude of the voltage applied to the transformer depends on the current flowing in the DC circuit. The resulting current ripple increases the stress on the DC circuit capacitors and semiconductor switching elements and reduces the efficiency of the converter.

Due to the relatively small leakage inductance, the phase delay  $\tau$  associated with the nominal power is only a few percent of the switching period,

which is generally comparable to the switching dead time occurring in the system (inserted dead time in the half-bridge control signal, turn-on and turn-off delay of semiconductor switching elements). Since the effective dead time depends on the operating parameters (temperature, current), direct compensation for the effect of dead time requires complicated and costly methods (lookup table, hardware based dead time measurement).

---

**1.1 Subthesis.** *[J1][C1] The ripple current control (RCC) algorithm, which utilizes current rate of change feedback, significantly reduces current stress caused by DC voltage measurement errors, thereby enhancing the converter's efficiency.*

---

The primary and secondary currents of the transformer shown in Figure 1 can be written in the following form:

$$I_P(s) = \underbrace{\frac{1}{s} \frac{L_m}{k} (U_P(s) - U'_S(s))}_{I_c} + \underbrace{\frac{1}{s} \frac{L'_{ss}}{k} U_P(s)}_{I_{pm}} \quad (6)$$

$$I'_S(s) = \underbrace{\frac{1}{s} \frac{L_m}{k} (U_P(s) - U'_S(s))}_{I_c} - \underbrace{\frac{1}{s} \frac{L_{sp}}{k} U'_S(s)}_{I_{sm}} \quad (7)$$

$$k = L_m(L_{sp} + L'_{ss}) + L_{sp} \cdot L'_{ss} \quad (8)$$

Based on equations (6) and (7), the primary and secondary currents of the transformer can be broken down into three components.  $I_c$  appears in both equations. Its value is zero in sections with the same polarity if the DC voltages are equal in magnitude. In this case, only two components remain, whose sum with opposite signs gives the magnetizing current of the transformer, so we refer to them as components  $I_{pm}$  and  $I_{sm}$ . If  $U_{DCP} \neq U'_{DCS}$ , then during the period of identical primary and secondary voltage polarity, the transformer current will also change due to  $I_c$ . If the transformer's stray inductance is low, even a small difference in DC voltages can result in significant current changes.

Ideally, the goal would be to minimize the current ripple of the transformer, i.e., only the magnetizing current should be present. Other considerations may also be taken into account, for example, if the magnetizing current is supplied only from the primary side, the AC component of the DC capacitor current on the secondary side can be significantly reduced.

Let  $q$  denote the fraction of the transformer's magnetizing current ( $I_m$ ) flowing on the secondary side, and let its range be  $[0,1]$ . The current component  $I_c$  can be changed by modifying the DC voltages, thus achieving

the desired value of  $q$ :

$$I_c = -qI_{pm} + (1-q)I_{sm} \quad (9)$$

The required DC voltage value can be obtained using equations (6), (7) and (9).

$$\frac{U'_S}{U_P} = \frac{L_m + qL'_{ss}}{L_m + (1-q)L_{sp}} \quad (10)$$

If the stray inductance of the transformer is much smaller than the magnetizing inductance, then a voltage difference comparable to the usual voltage detection accuracy (1%) may be sufficient to achieve the desired effect. Therefore, it is advisable to supplement the SPS control loop with an additional PI controller (see Figure 4). The  $q$  value required for feedback can be calculated based on the primary and secondary currents of the transformer.

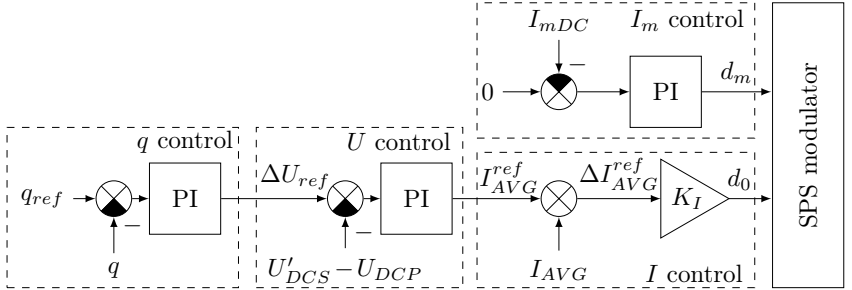


Figure 4: The control diagram of RCC.

I verified the operation of the method using HIL simulation and measurements on real hardware. The simulation waveforms are shown in Figure az 5. Using RCC, the peak value of the transformer current was reduced, allowing the converter to operate with higher efficiency. The value of  $q$  can be any value between 0 and 1, so the magnetizing current can be transferred to the primary or secondary side as needed.

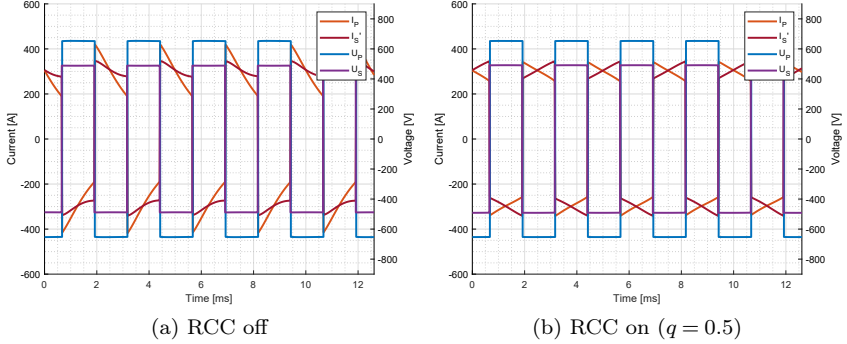


Figure 5: Simulation result with and without RCC.

---

**1.2 Subthesis.** [B1] [J2] I demonstrated that switching dead time leads to discontinuous current conduction in SPS controlled DAB converters. To address this, I introduced a novel adaptive dead time compensation (ADTC) logic that effectively eliminates the adverse effects of switching dead time in such systems and the error of the current regulation is significantly reduced.

---

Due to switching dead times, when switching the half-bridges of SPS-controlled DAB converters, the voltage-time area reaching the transformer will differ from the value desired by the controller. Depending on the current of the given half-bridge before and after switching, three situations may arise.

If the current flow remains continuous during the switchover, only the difference between the secondary and primary side switch-off delays causes a problem. In this case, the width of the voltage pulse connected to the transformer's leakage inductance is:

$$\tau_{CCCM} = \tau_{orig} + t_{off}^S - t_{off}^P \quad (11)$$

If the current drops to zero when switching the primary side half-bridge, discontinuous conduction will occur. In this case, the pulse width depends on several converter parameters:

$$\tau_{DCCMP} = \tau_{orig} + t_{off}^S - t_d - t_{on}^P - (L_{sp} + L'_{ss}) \frac{|I_P|}{U_{DCP} + U'_{DCS}} \quad (12)$$

If the transformer current drops to zero when the secondary side switches are switched, secondary side discontinuous conduction occurs. In this case,

the pulse width of the voltage is determined by the transformer's leakage inductance and current, as well as the DC voltages:

$$\tau_{DCCMS} = (L_{sp} + L'_{ss}) \frac{|I_P|}{U_{DCP} + U'_{DCS}} \quad (13)$$

In order to eliminate the effects of dead time, in addition to the instantaneous value of the primary current, we need to know the delay values and system parameters appearing in the equations. Implementing this can be difficult, so it is better to use an adaptive method.

The control loop is shown in Figure 6. In each switching period, before and after the half-bridges are switched, we measure the change in the average current of the transformer ( $\Delta I_{AVG}$ ) and subtract it from the reference value corresponding to the change. The resulting error signal is integrated and the output of the integrator is added to the output of the original current regulator. Due to the magnetizing current of the transformer, different dead times may occur during the two switching operations within a switching period. For this reason, two independent integrators are used.

By using dead time compensation, the  $\Delta I_{AVG}^{ref}$  signal becomes proportional to the power flowing through the converter. This improves the dynamic behavior of the converter and is essential for the proper operation of the algorithm described in Subthesis 2.1.

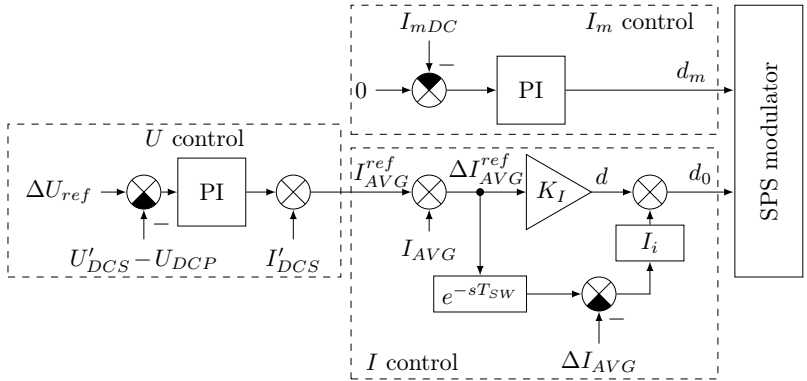


Figure 6: Control diagram of the SPS adaptive dead time compensation.

---

**2 Thesis.** [J3] [J4] [C2] [C3] [C4] *I have proposed two new control techniques, which improves the dynamic behavior of DAB converters. With the cross-period single phase shift (CP-SPS) control the duration of voltage transients can be significantly reduced using load current forward feed and in-period switching actions. With the continuous cross-period single phase shift (CCP-SPS) control, the voltage regulation loop delay can be reduced, thus, during a load transients, the DC bus voltage swing amplitude is reduced compared to regular SPS control. I have shown how the switch delays affect the CP-SPS and CCP-SPS control techniques. I have proposed an adaptive dead time compensation (ADTC) method, which eliminates the transformer current waveform anomalies, using feedback from the transformer current change.*

---

In power supplies, including DAB converters, it is important that the output voltage does not change significantly in response to sudden load current changes. In regulated power converters, a transient voltage can be observed in such cases, which settles depending on the parameters of the control loop. In SPS-controlled DAB converters, the two DC voltages always tend to equalize, thus potentially offering good dynamic characteristics. However, the current in the semiconductors can increase significantly if the voltage difference between the two DC voltages becomes too large.

---

**2.1 Subthesis.** [C2] [C3] [C4] *I have proposed the cross-period single phase shift (CP-SPS) control, which significantly reduces the duration of voltage transients on a sudden load change event, using load current forward feed and in-period switching actions.*

---

With SPS control, we can only influence the current flowing through the transformer dispersion twice within a switching period. The basic idea behind CP-SPS control is to intervene several times during a switching period, if necessary, thereby improving the dynamic behavior of the control loop. The switching period is divided into 6 phases (PH1-PH6) and we intervene once in each phase.

Figure 7 shows the possible switching events within the period. For example, in the third phase of the first switching period, the primary transformer voltage is inverted for a time  $\tau_{action}^{IA}$ . This causes the following change in the average current of the transformer:

$$\Delta I_{AVG}^{inv} = \tau_{action}^{IA} \cdot \frac{U_{DCP} + U'_{DCS}}{L_{sp} + L'_{ss}} \quad (14)$$

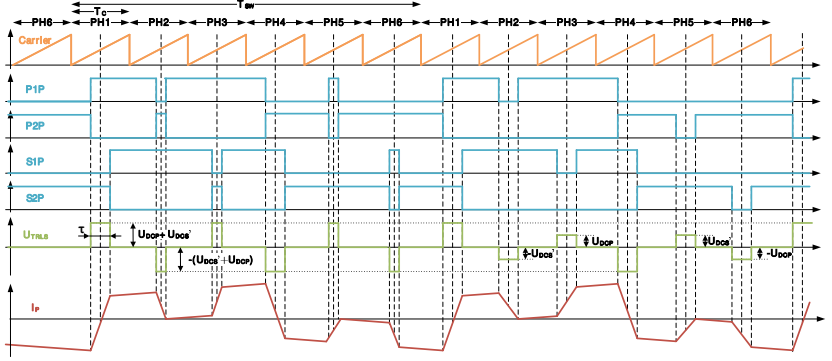


Figure 7: CP-SPS control waveforms illustrating possible current modifications.

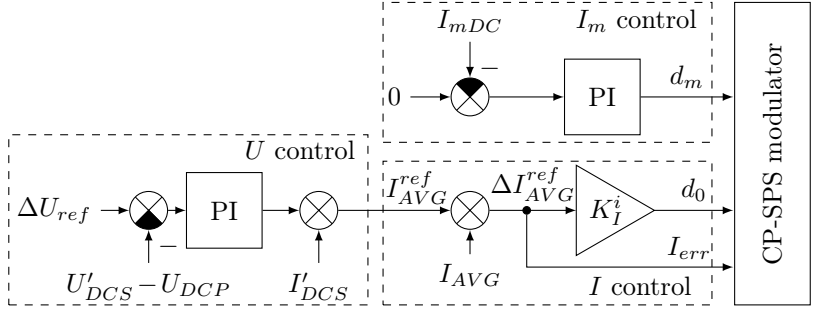


Figure 8: Control diagram of the CP-SPS algorithm.

In the second and third phases of the second switching period, the primary and secondary coils are short-circuited. In this case, the current surge is approximately half that of the inversion.

$$\Delta I_{AVG}^{PSA} = \tau_{action}^{PSA} \cdot \frac{U'_{DPCS}}{L_{sp} + L'_{ss}} \quad (15)$$

$$\Delta I_{AVG}^{SSA} = \tau_{action}^{SSA} \cdot \frac{U_{DCP}}{L_{sp} + L'_{ss}} \quad (16)$$

The advantage of this solution is that we only need to switch one half-bridge, so the switching loss will be lower than with inversion.

The modified SPS control loop is shown in Figure 8, and the switching table is shown in Table 2. An important change compared to SPS control is that we feedforward with the converter output DC current. The voltage

Table 2: CP-SPS modulator switching table.

	PH1	PH2 and PH5		PH3 and PH6		PH4
		$I_{err} > 0$	$I_{err} \leq 0$	$I_{err} > 0$	$I_{err} \leq 0$	
P1 to $U_{DCP}$	$\frac{1-d_0}{2} - d_m$	x	$\frac{1+d_0}{2}$	x	x	x
P1 to 0	x	x	$\frac{1-d_0}{2}$	x	x	$\frac{1-d_0}{2} + d_m$
P2 to $U_{DCP}$	x	x	x	x	$\frac{1+d_0}{2}$	$\frac{1-d_0}{2} + d_m$
P2 to 0	$\frac{1-d_0}{2} - d_m$	x	x	x	$\frac{1-d_0}{2}$	x
S1 to $U_{DCS}$	$\frac{1+d_0}{2} - d_m$	$\frac{1+d_0}{2}$	x	x	x	x
S1 to 0	x	$\frac{1-d_0}{2}$	x	x	x	$\frac{1+d_0}{2} + d_m$
S2 to $U_{DCS}$	x	x	x	$\frac{1+d_0}{2}$	x	$\frac{1+d_0}{2} + d_m$
S2 to 0	$\frac{1+d_0}{2} - d_m$	x	x	$\frac{1-d_0}{2}$	x	x

regulator continues to run only in phases PH1 and PH4. The current regulator feedback ( $I_{FB}^i$ ) and  $K_I^i$  have different values in each phase. The switching table shows that we intervene in the phases during the period if the average current of the transformer deviates from the output of the voltage regulator.

I checked the control method with HIL simulation. Figure 9 clearly shows that during large power changes (the sign of the power also changes), the SPS control is unable to limit the converter current, causing the over-current protection to trip at 900 A. In contrast, with CP-SPS control, much smaller changes in the output DC voltage can be seen after the load step.

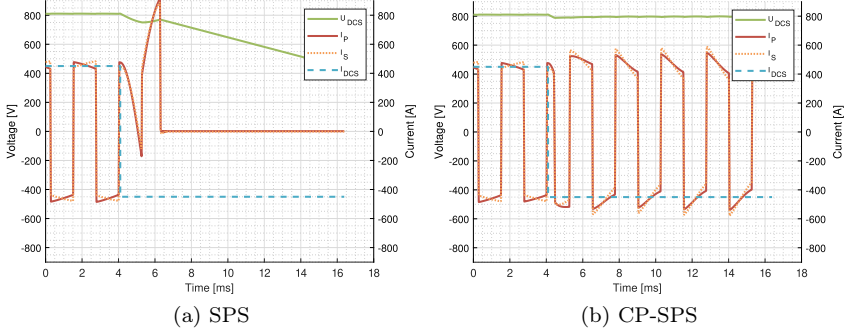


Figure 9: Simulation results of SPS and CP-SPS control.

---

**2.2 Subthesis.** [J4] I have proposed the continues cross-period single phase shift (CCP-SPS) control, which reduces the voltage regulation loop delay, therefore the DC bus voltage swing amplitude is reduced during load transients, compared to SPS control.

---

In CP-SPS control, the converter output current is fed forward in the control loop. This can result in oscillations if a series LC circuit is connected to the converter output. This can occur, for example, if another switching power supply is connected to the load. The inductance of the connecting cable between the two converters and the input capacitor of the load power supply form the LC circuit.

Another problem with CP-SPS control is that, if the current error is small, the pulse width required for intervention is comparable to the switching dead time. For this reason, in practice, we must define a minimum intervention time, below which we do not perform switching within the period.

CCP-SPS control is a further development of the CP-SPS method, in which no feedforward is required. The possible switching actions are shown in Figure a 10. In all cases, we intervene on both the primary and secondary sides for a  $\tau_{max}$  time duration in all in-period phases. To modify the transformer current, we apply a delay between the start of the interventions on the primary and secondary sides.

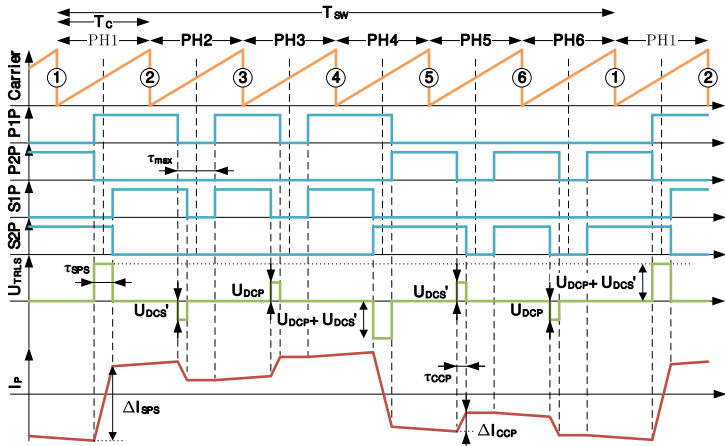


Figure 10: CCP-SPS control resulting waveforms, illustrating possible in-period switching actions.

In the control loop (Figure 11), the only thing required in addition to SPS control is to use the current error in the switching table (Table 3). An important change is that the voltage regulator can be run in all phases, thus reducing the delay of the control loop to approximately one third.

I tested the CCP-SPS control with a 360kW DAB converter. The measurement results are shown in Figure 12. The load current jumped from 0 A to 250 A. It can be clearly seen that with CCP-SPS control, both the decay time and amplitude of the transient in the secondary voltage are significantly reduced compared to SPS control.

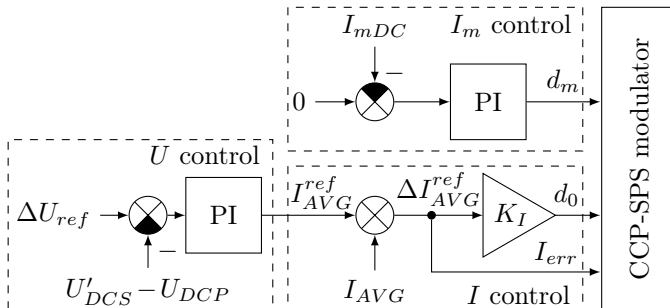


Figure 11: Control diagram of the CCP-SPS algorithm.

Table 3: CCP-SPS modulator switching table.

	PH1	PH2 and PH3		PH5 and PH6		PH4
		$I_{err} > 0$	$I_{err} \leq 0$	$I_{err} > 0$	$I_{err} \leq 0$	
P1 to $U_{DCP}$	$\frac{1-d_0}{2} - d_m$	$\frac{1+d_{max}}{2}$	$\frac{1+d_{max}}{2}$	x	x	x
P1 to 0	x	$\frac{1-d_{max}}{2} + d_0$	$\frac{1-d_{max}}{2}$	x	x	$\frac{1-d_0}{2} + d_m$
P2 to $U_{DCP}$	x	x	x	$\frac{1+d_{max}}{2}$	$\frac{1+d_{max}}{2}$	$\frac{1-d_0}{2} + d_m$
P2 to 0	$\frac{1-d_0}{2} - d_m$	x	x	$\frac{1-d_{max}}{2} + d_0$	$\frac{1+d_{max}}{2}$	x
S1 to $U_{DCS}$	$\frac{1+d_0}{2} - d_m$	$\frac{1+d_{max}}{2}$	$\frac{1+d_{max}}{2}$	x	x	x
S1 to 0	x	$\frac{1-d_{max}}{2}$	$\frac{1-d_{max}}{2} + d_0$	x	x	$\frac{1+d_0}{2} + d_m$
S2 to $U_{DCS}$	x	x	x	$\frac{1+d_{max}}{2}$	$\frac{1+d_{max}}{2}$	$\frac{1+d_0}{2} + d_m$
S2 to 0	$\frac{1+d_0}{2} - d_m$	x	x	$\frac{1-d_{max}}{2}$	$\frac{1+d_{max}}{2} + d_0$	x

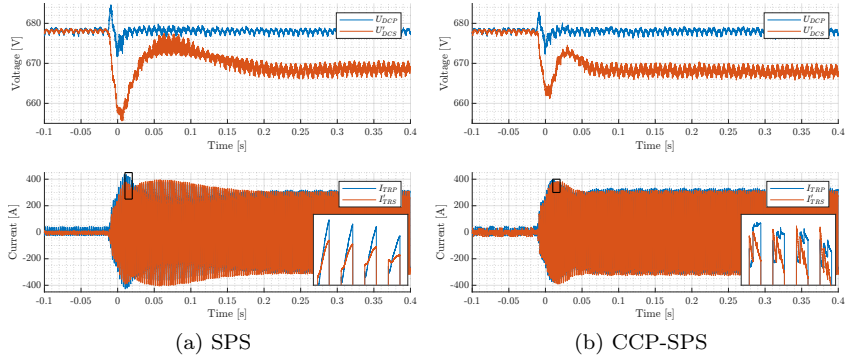


Figure 12: Measurement results using (a) SPS and (b) CCP-SPS control.

---

**2.3 Subthesis.** [J3] *I have proposed an adaptive dead time compensation (ADTC) method for the CCP-SPS control, which eliminates the transformer current waveform anomalies using feedback from the transformer current change.*

---

In CCP-SPS control, we intervene for at least  $\tau_{max}$  in each phase, which is usually comparable to the switching dead time. To achieve proper operation, the effects of the dead time must be compensated.

As a first step, I analyzed the effects of dead time in different states of the converter. As a result, it can be concluded that in continuous operation, the voltage-time area of the transformer’s leakage inductance increases or decreases by a factor of twice the effective dead time, depending on the sign of the current change. Therefore, in principle, the effect of dead time can be compensated for if the effective dead time is known.

Switching delays depend on the operating status of the converter (temperature, current), so an adaptive compensation solution is recommended. The control loop is shown in Figure 13. In each phase, the average transformer current before and after switching is measured. The measured current change is subtracted from the current change specified by the voltage regulator, and the resulting error signal is fed to an integrating controller. The estimated effective dead time is added to the output of the integrator, so that the controller only has to make corrections due to the uncertainty of the estimate. The exact times of the switching events are determined by  $d_0$  and  $d_c$ .

I verified the effectiveness of the method using HIL simulation. In the semiconductor model, I reduced the turn-off delay from 3  $\mu$ s to 40 ns during

converter operation. The simulation waveforms are shown in Figure 14. It can be observed that with the change in delay, the transformer current changes unnecessarily in in-period phases. The adaptive controller settles in approximately 100 ms time, at which point the amplitude of the current transients is significantly reduced.

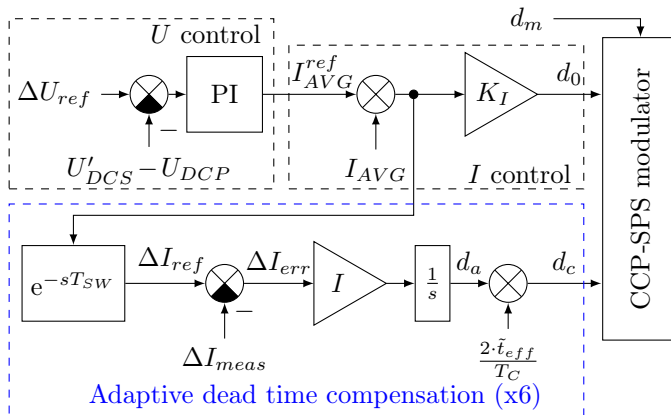


Figure 13: The CCP-SPS control diagram with adaptive dead time compensation.

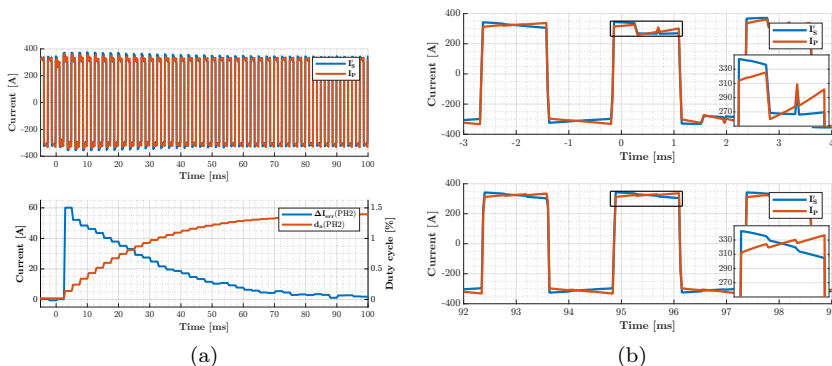


Figure 14: CCP-SPS simulation results with dead time compensation.

---

**3 Thesis.** *[C5] I have proposed a startup technique for low frequency DAB converters equipped with low leakage inductance, which allows peak current limited operation. I have shown how the precharge time could be estimated and the resulting equation was validated with HIL simulation.*

---

Starting DAB converters is not a trivial task if the reduced voltages of the two DC buses differ significantly. Due to the voltage difference, a high current may develop across the transformer, which can damage the main circuit components. The essence of the precharge method I proposed is that at start-up, only one of the transformer's H-bridges is operated, while the other is used as a diode rectifier, and a symmetrical square wave with variable pulse width is generated on the switched side.

Let us assume that the entire bridge is operated on the primary side of the transformer. By measuring the voltage of the DC buses and knowing the stray inductance of the transformer, the pulse width corresponding to the peak current of the transformer primary ( $\hat{I}_P$ ) can be calculated.

$$\tau_{pulse} = \hat{I}_P \cdot \frac{L_{sp} + L'_{ss}}{U_{DCP} - U'_{DCS}} \quad (17)$$

In each switching period, we calculate the required duration and use it to charge the secondary side capacitor with a constant peak current. The converter then operates in a pulsed mode. The precharging process can be further accelerated by applying voltage to the primary winding of the transformer again after the current has dropped to zero, but this would result in a variable switching frequency.

It can be shown that discontinuous current conduction at a constant peak current is only possible if the secondary side DC voltage lies within a certain range. Based on this, the precharging process can be divided into three phases: early, intermediate, and final. The boundaries of these phases can be calculated based on the waveforms of the main circuit. In each phase, the duration required for precharging can be determined in a different manner.

The effectiveness of the precharge method was verified using HIL simulation. The transformer waveforms are shown in Figure 15. The discontinuous conduction of the converter can be observed, as well as how the primary current of the transformer decreases with increasing secondary voltage. The transition to normal regulated operation can be achieved with virtually no transients, as shown in the figure.

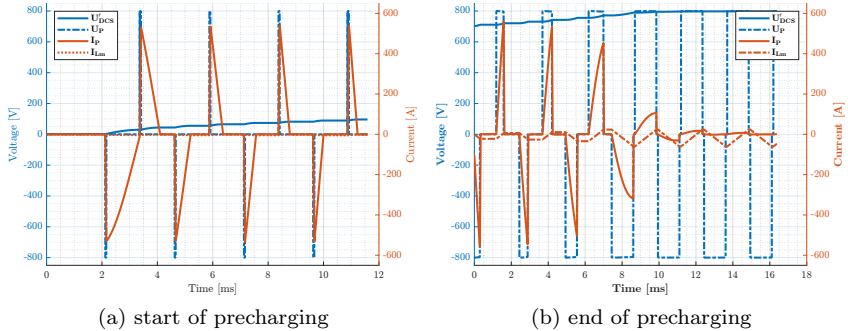


Figure 15: Simulation waveforms recorded during precharging.

## 4 Practical applications

An important goal of the research was the practical application of the results. Accordingly, the solutions developed form an integral part of the control software for the DAB converter of the power electronics laboratory built as part of the FIEK 16-1-2016-0007 project. My solutions are not limited to this specific device, but can be widely applied to DAB topologies.

## Journals

- [J1] **Szabolcs Veréb**, László Stranyóczy, Zoltán Sütő, and Attila Balogh, “Ripple current control for single phase-shift dual active bridge converters,” *Renewable Energy & Power Quality Journal (RE&PQJ)*, vol. 22, pp. 76–84, Sept. 2024.
- [J2] **Szabolcs Veréb**, András Futó, Zoltán Sütő, Attila Balogh, and István Varjasi, “Adaptive dead time compensation for cross-period single phase shift control of dual active bridge converters,” *Renewable Energy & Power Quality Journal (RE&PQJ)*, vol. 18, pp. 327–332, June 2020.
- [J3] **Szabolcs Veréb**, András Futó, Zoltán Sütő, Attila Balogh, and István Varjasi, “Adaptive dead time compensation for continuous cross-period single phase shift control of dual active bridge converters,” *Renewable Energy & Power Quality Journal (RE&PQJ)*, vol. 20, pp. 256–262, Sept. 2022.
- [J4] **Szabolcs Veréb**, András Futó, Zoltán Sütő, Attila Balogh, and István Varjasi, “Continuous cross-period single phase shift control for dual active bridge converters,” *Renewable Energy & Power Quality Journal (RE&PQJ)*, vol. 19, pp. 222–228, Sept. 2021.

## Conference Proceedings

- [C1] **Szabolcs Veréb**, “Adaptive single phase shift control of dual active bridge converters,” in *Proceedings of the Automation and Applied Computer Science Workshop 2022 (AACCS’22)*, pp. 9–19, 2022.
- [C2] **Szabolcs Veréb**, “Deadtime effects on in-period switching actions in cross-period single phase shift control of dual active bridge converters,” in *Proceedings of the Automation and Applied Computer Science Workshop 2021: AACCS’21*, 2021.
- [C3] **Szabolcs Veréb** and István Varjasi, “DAB teljesítmény átalakító alkalmazása a BME moduláris hibrid hajtáslánc laboratóriumában,” in *XI. Mechwart András Ifjúsági Találkozó*, pp. 118–127, 2021.
- [C4] **Szabolcs Veréb**, András Futó, Zoltán Sütő, Attila Balogh, and István Varjasi, “Cross-period single phase shift control technique for high power and low frequency dual active bridge converters,” in *2019 International Conference on Electrical Drives & Power Electronics (EDPE)*, pp. 385–390, IEEE, 2019.
- [C5] **Szabolcs Veréb** and Dávid Kiss, “Advanced precharge control for high power low frequency dual active bridge converters,” in *Applied Computer Science Workshop (AACCS)*, 2019.

## Book Chapters

- [B1] **Szabolcs Veréb**, *Trends in renewable energy and power quality*, ch. Adaptive dead time compensation for dual active bridge converters, pp. 314–326. Cambridge Scholars Publishing, 2024.

## Publications not related to the theses

- [M1] **Szabolcs Veréb**, Gergely G. Balázs, Tamás Kökényesi, Zoltán Sütő, and István Varjasi, “Application dependent optimization of balancing methods for lithium-ion batteries,” in *2018 IEEE 18th International Power Electronics and Motion Control Conference (PEMC)*, pp. 223–228, IEEE, 2018.
- [M2] Tamas Kokenyesi, Marton Hegedus, **Szabolcs Vereb**, Attila Balogh, Zoltan Suto, and Istvan Varjasi, “FPGA-driven DAC with second order sliding mode control of filter model for hardware-in-the-loop simulators,” in *2018 IEEE 18th International Power Electronics and Motion Control Conference (PEMC)*, pp. 824–829, IEEE, 2018.

- [M3] Zoltán Sütő, Attila Balogh, Dávid Kiss, **Szabolcs Veréb**, and István Varjasi, “Power HIL emulation of AC machines with parallel connected ANPC bridge arms,” in *2018 IEEE 18th International Power Electronics and Motion Control Conference (PEMC)*, pp. 592–598, IEEE, 2018.
- [M4] **Szabolcs Veréb**, “Correlation of control hardware, applied control method and dynamic behavior of a NPC three-level inverter,” in *Applied Computer Science Workshop (AACS)*, 2018.
- [M5] **Szabolcs Veréb**, “Avoiding grid current oscillations in power factor correction boost converter,” in *Proceedings of the Automation and Applied Computer Science Workshop 2020*, pp. 22–32, 2020.
- [M6] László Stranyóczy, **Szabolcs Veréb**, and Zoltán Sütő, “Feszültségkiegyenlítő módszerek alkalmazása hétszintű inverterben,” *ELEKTROTECHNIKA*, vol. 115, 2022/3-4, pp. 5–9, 2022.
- [M7] Bálint Palásti, **Szabolcs Veréb**, and András Futó, “Háromfázisú hálózatra csatlakoztatott inverterek hatásfokának növelése és aszimmetria kompenzációja egy fázis tranziensmentes lekapcsolásával,” in *XII. Mechwart András Ifjúsági Találkozó*, p. 102, 2022.
- [M8] László Stranyóczy, András Futó, **Szabolcs Veréb**, István Varjasi, and Zoltán Sütő, “Peak current mode control for grid-connected energy storage inverters,” *Renewable Energy & Power Quality Journal (RE&PQJ)*, vol. 22, pp. 132–136, Sept. 2024.



